Supplementary Information for

Recent ice melt above a mantle plume track is accelerating the uplift of Southeast Greenland

Maaike F. M. Weerdesteijn* and Clinton P. Conrad

*Corresponding author. Email: maaikew@unis.no

This PDF file includes:

- Figures S1 to S22
- Tables S1 to S3
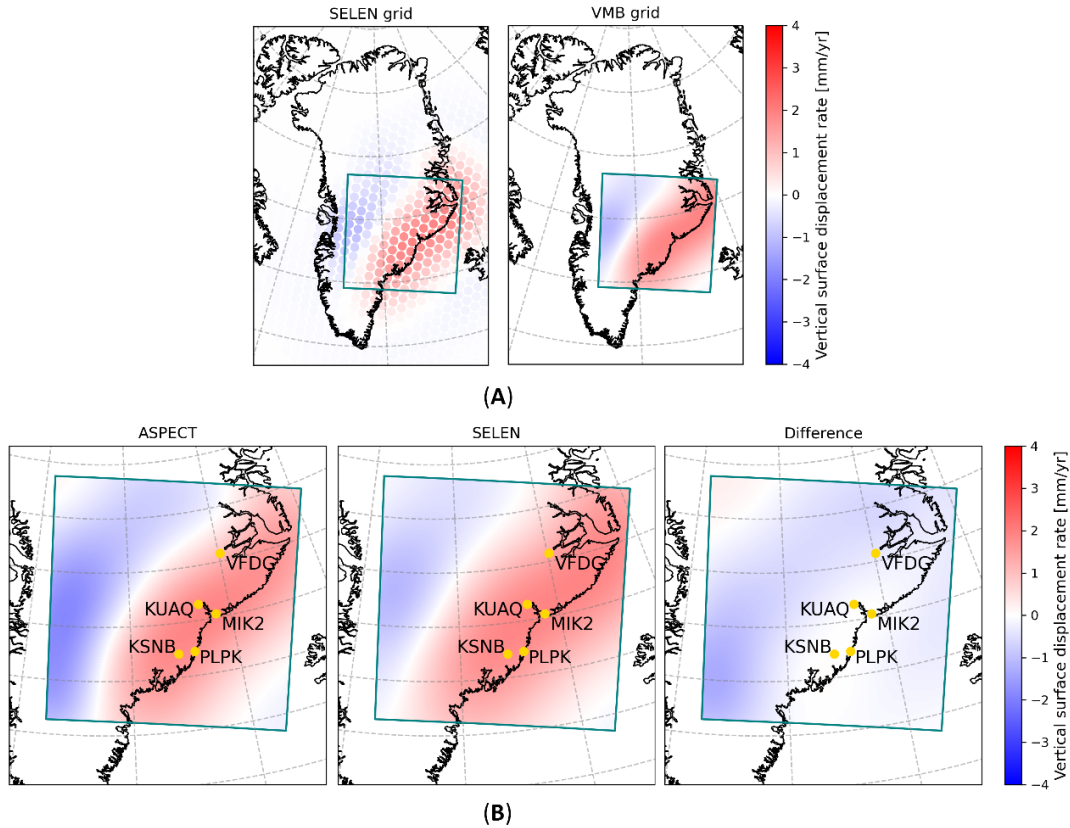
Fig. S1. Comparison of present-day uplift rates, computed for last glacial cycle loading using regional (ASPECT) and global (SELEN) modelling approaches.

(**A**) The model vertical displacement rate (left, as in Fig. S20D) and interpolated onto the VMB grid (right), computed for the last glacial cycle ice loading changes within the ice loading area (Fig. S5) using the global modelling approach in SELEN [1]. (**B**) The vertical surface displacement rate for the same ice loading changes computed using the regional modelling approach in ASPECT (left), the global modelling approach in SELEN (middle, as right panel of **A**), and the difference between them (right), with the five GNSS sites (yellow dots) and the ice loading area (teal box).

Table S1. Present-day uplift rates in southeast Greenland, computed for loading changes of the last glacial cycle (Fig. S5) using the regional (ASPECT) and global (SELEN) modelling approaches at the five GNSS sites and the difference between them (Fig. S1B).

GNSS station	ASPECT [mm/yr]	SELEN [mm/yr]	Difference [mm/yr]
KUAQ	1.84	1.88	-0.05
MIK2	1.89	1.89	0.00
PLPK	1.71	1.71	0.00
KSNB	1.81	1.78	0.03
VFDG	0.97	1.35	-0.38

2
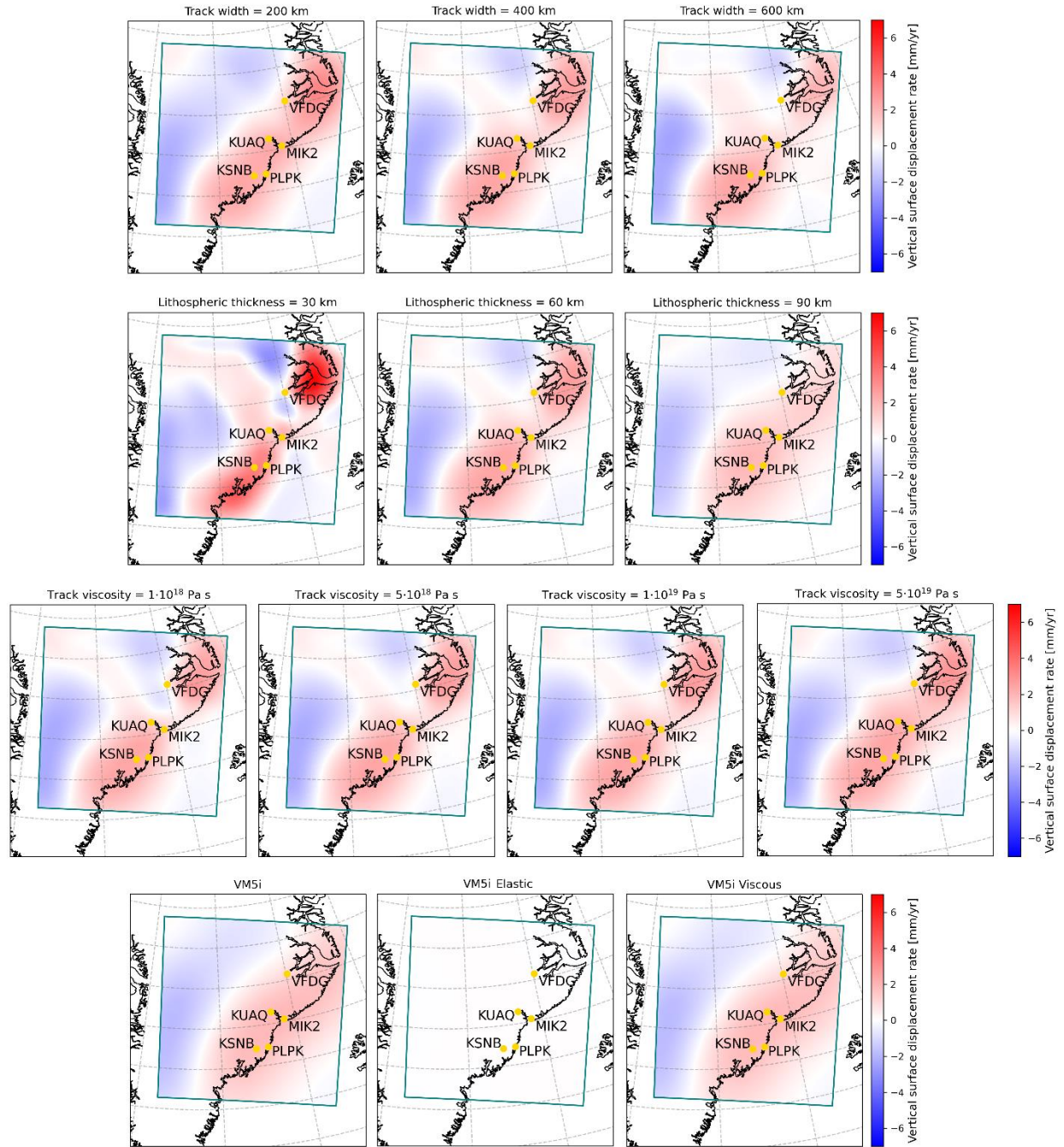
Fig. S2. Regional modelling of present-day uplift rates in response to the last glacial cycle ice loading within the ice loading area, for different plume track models.

Different Earth models are shown, as described in Fig. 4.

Table S2. Present-day vertical displacement rates at the five GNSS sites in response to global models of (i) last glacial cycle ice loading changes and (ii) the elastic response following contemporary ice loading changes over Greenland, and regional models of Earth's response following ice loading changes over the (iii) last glacial cycle, (iv) second millennium, and (v) the satellite altimetry era. For regional models (iii, iv, v), the range of rates for varying elastic thickness, track width, and track viscosity are given. The sum of these rates can be compared to (vi) GNSS observations, as measured in Fig. S19.

Vertical surface displacement rate [mm/yr]	KUAQ	MIK2	PLPK	KSNB	VFDG
i. Global: last glacial cycle	-2.20	-2.18	-2.47	-2.56	-1.78
ii. Greenland: elastic	0.88	0.82	0.87	0.93	0.85
iii. Regional: last glacial cycle (average)	0.96-2.09 (1.44)	1.00-2.17 (1.53)	1.72-2.91 (2.08)	1.85-3.45 (2.42)	0.00-1.01 (0.48)
iv. Regional: second millennium	0.79-14.18	0.13-5.25	0.07-1.68	0.11-0.88	0.01-3.35
v. Regional: satellite altimetry era	2.03-34.94	0.65-7.78	0.49-1.88	0.91-2.35	0.47-4.00
vi. GNSS observations	17.44±1.10	12.39±0.83	9.70±0.82	12.85±0.68	4.95±0.73
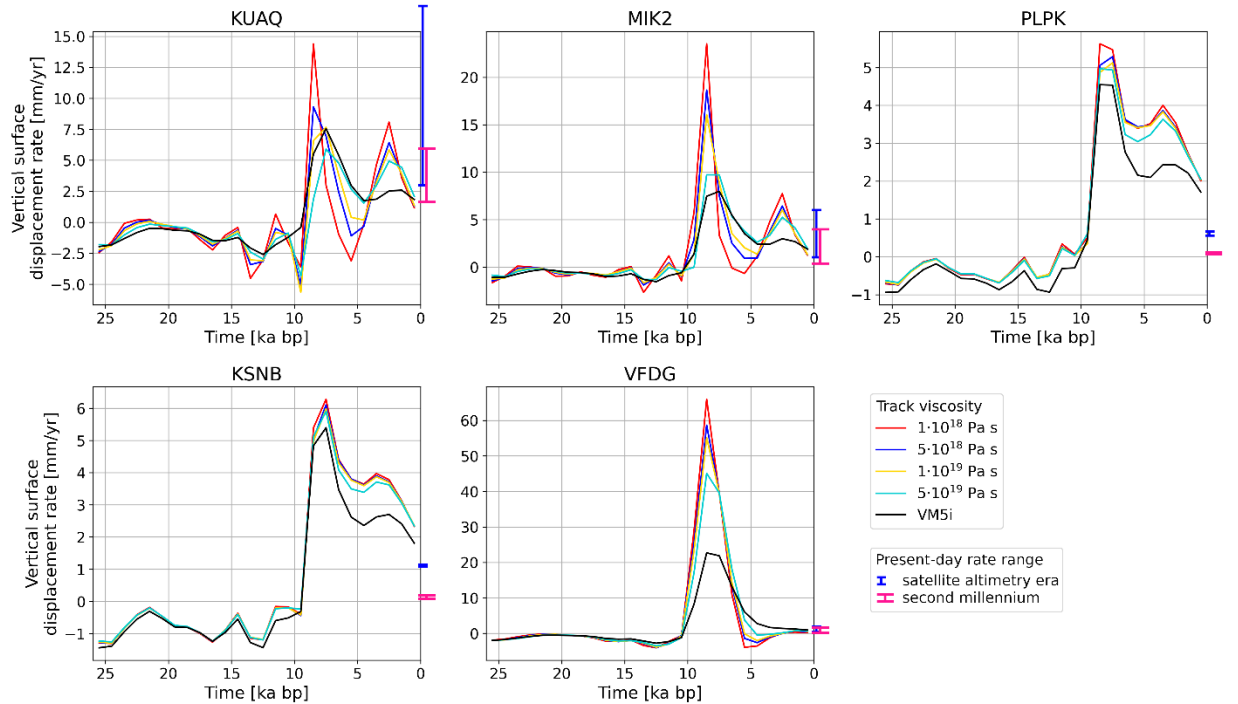
(A)
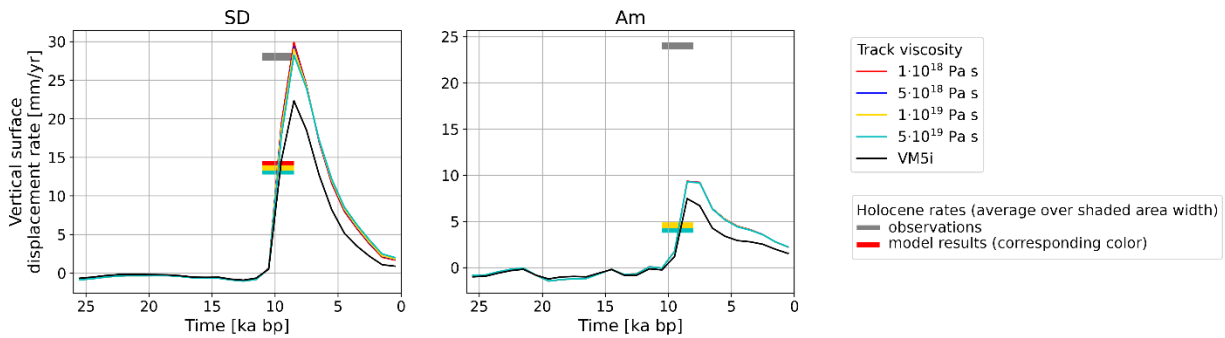
(B)

Fig. S3. Uplift rates due to last glacial cycle ice loading for different plume track viscosities. Vertical surface displacement rates since the last glacial maximum for track viscosities of $1\cdot10^{18}$ Pa s (red), $5\cdot10^{18}$ Pa s (blue), $1\cdot10^{19}$ Pa s (yellow), $5\cdot10^{19}$ Pa s (cyan), a plume track width of 400 km and a lithospheric thickness of 60 km outside the plume track, **(A)** for the five GNSS sites and **(B)** for the two sea level sites. Shown for comparison are results for the layered VM5i rheological model (black), ranges of present-day rates induced by ice loading changes over the satellite altimetry era (blue bar) and second millennium (pink bar) in (A), and ranges of Holocene uplift rates based on observations (grey bar) and model results (colored bars) in (B), for the Earth models with a plume track considered here.

(A)

(B)
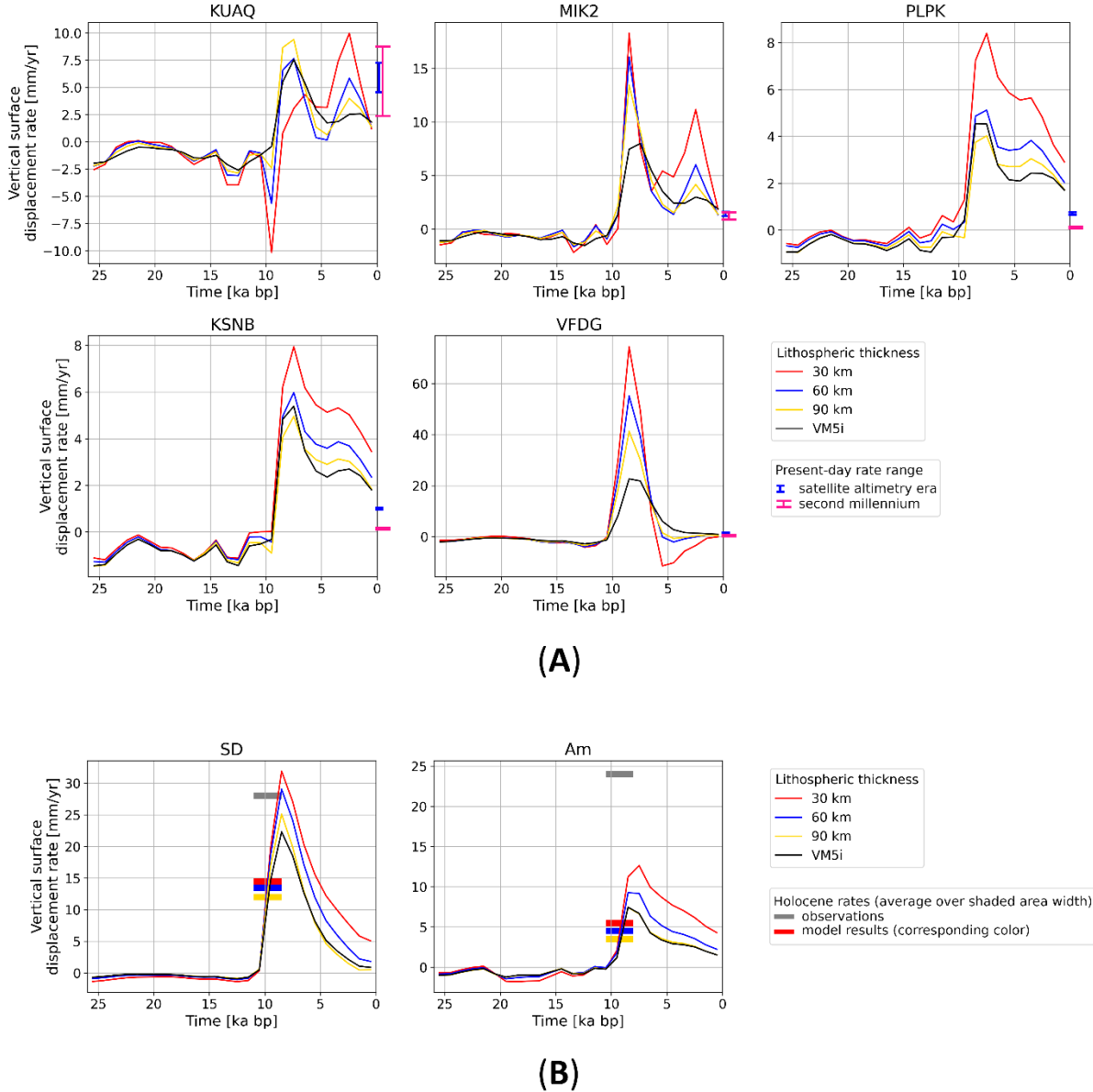
Fig. S4. Uplift rates due to last glacial cycle ice loading for different lithospheric thicknesses.

Vertical surface displacement rates since the last glacial maximum for lithospheric thicknesses of 30 km (red), 60 km (blue), 90 km (yellow) outside the plume track, a plume track width of 400 km and a track viscosity of $1 \cdot 10^{19}$ Pa s, **(A)** for the five GNSS sites and **(B)** for the two sea level sites. Shown for comparison are results for the layered VM5i rheological model (black), ranges of present-day rates induced by ice loading changes over the satellite altimetry era (blue bar) and second millennium (pink bar) in (A), and ranges of Holocene uplift rates based on observations (grey bar) and model results (colored bars) in (B), for the Earth models with a plume track considered here.
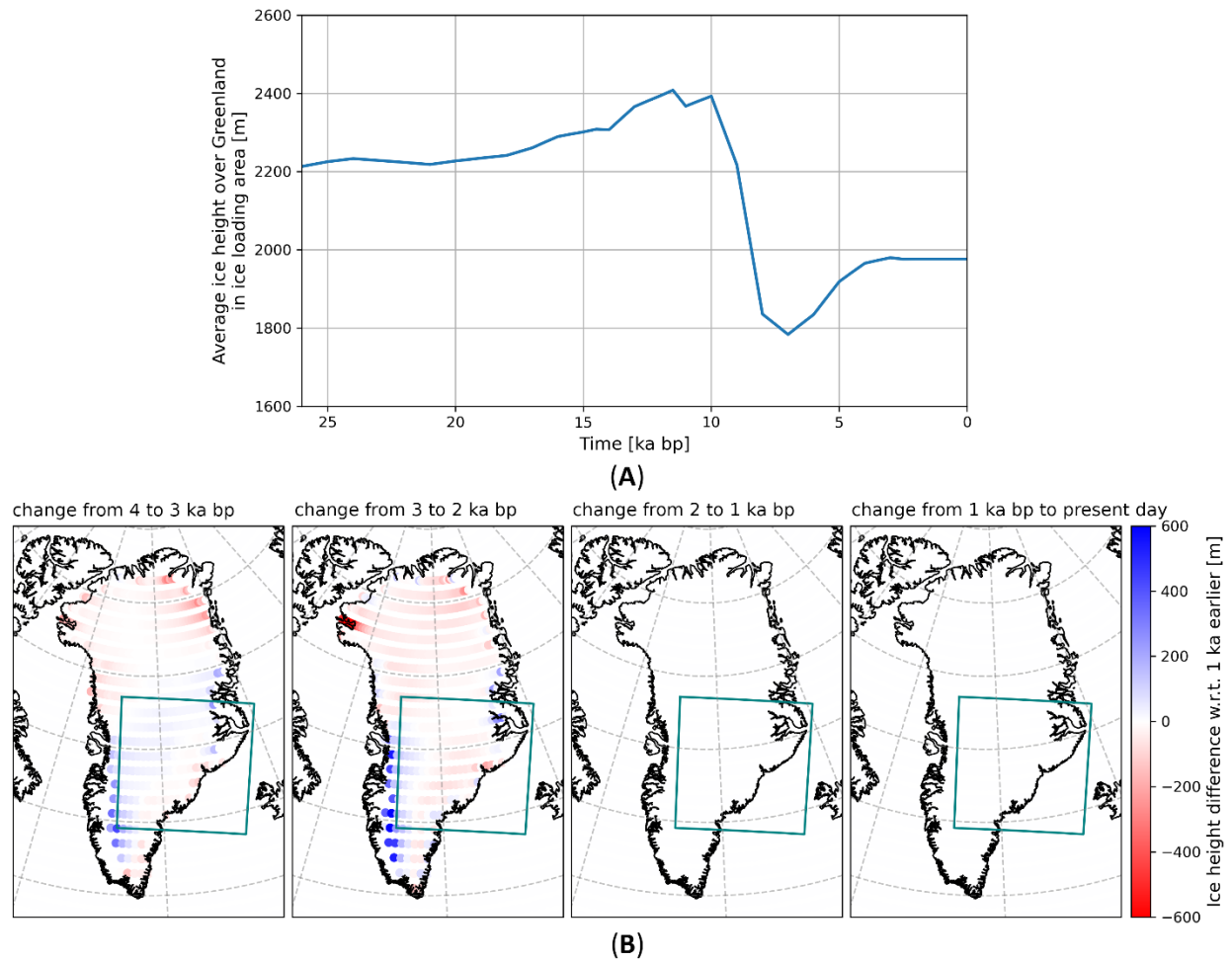
Fig. S5. Ice height evolution of the ICE-6G_C ice history model.
(**A**) Average ice height of the ICE-6G_C ice history model [2, 3] within the ice loading area in southeast Greenland as function of time. (**B**) Changes in ice height for the ICE-6G_C ice history model across Greenland during each of the last 4 millennia, with the ice loading area (teal box).
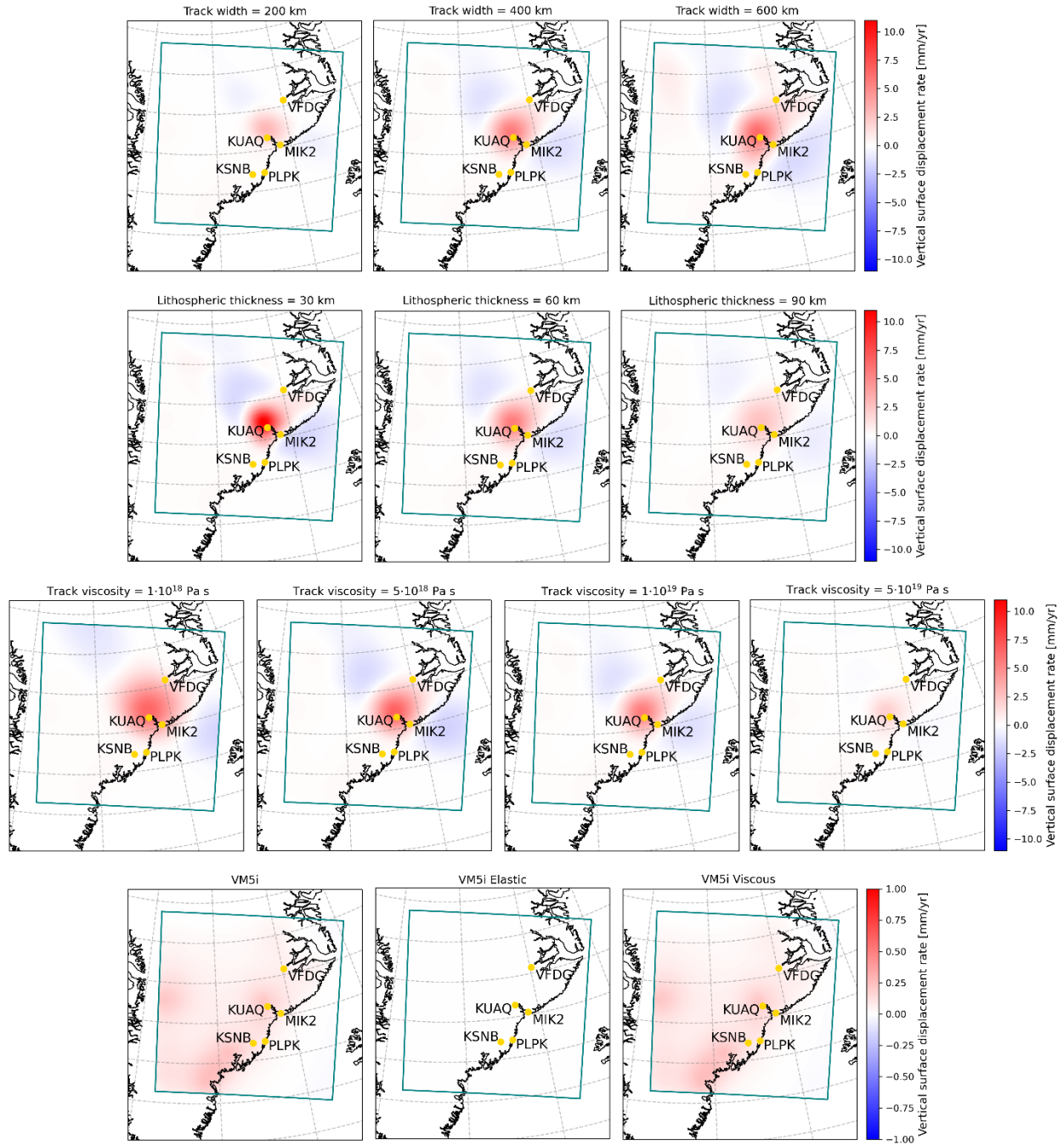
Fig. S6. Regional modelling of present-day uplift rates in response to second millennium ice loading changes within the ice loading area, for different plume track models.

Different Earth models are shown, as described in Fig. 4.
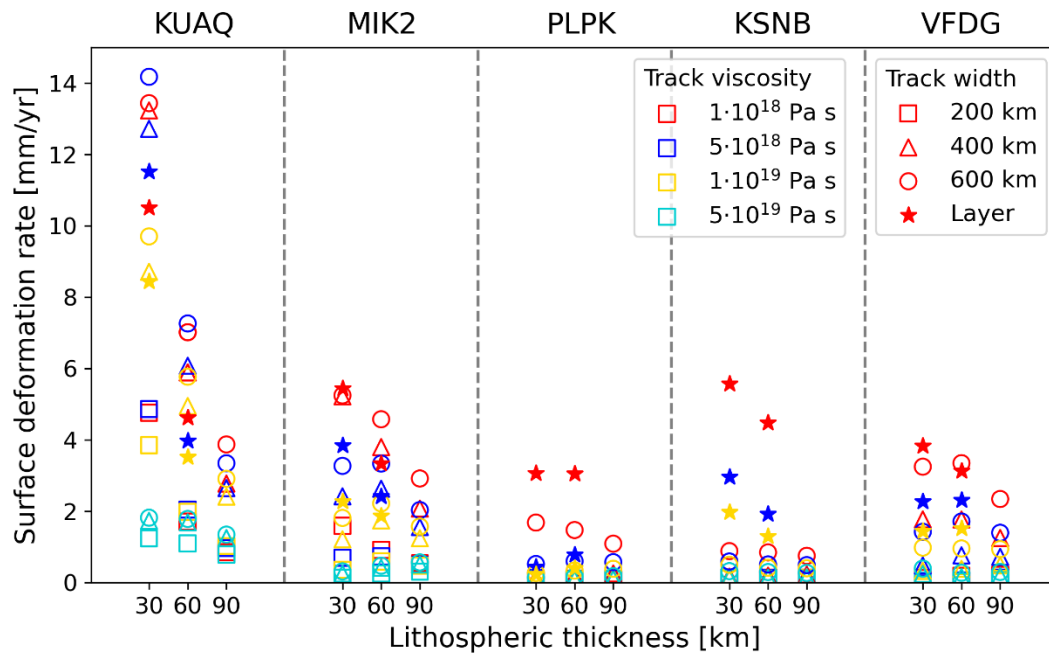
Fig. S7. Uplift rates at the five GNSS sites in response to the second millennium ice loading changes (only) for different plume track models.

Like Fig. 5, but showing uplift in response to second millennium ice loading changes.
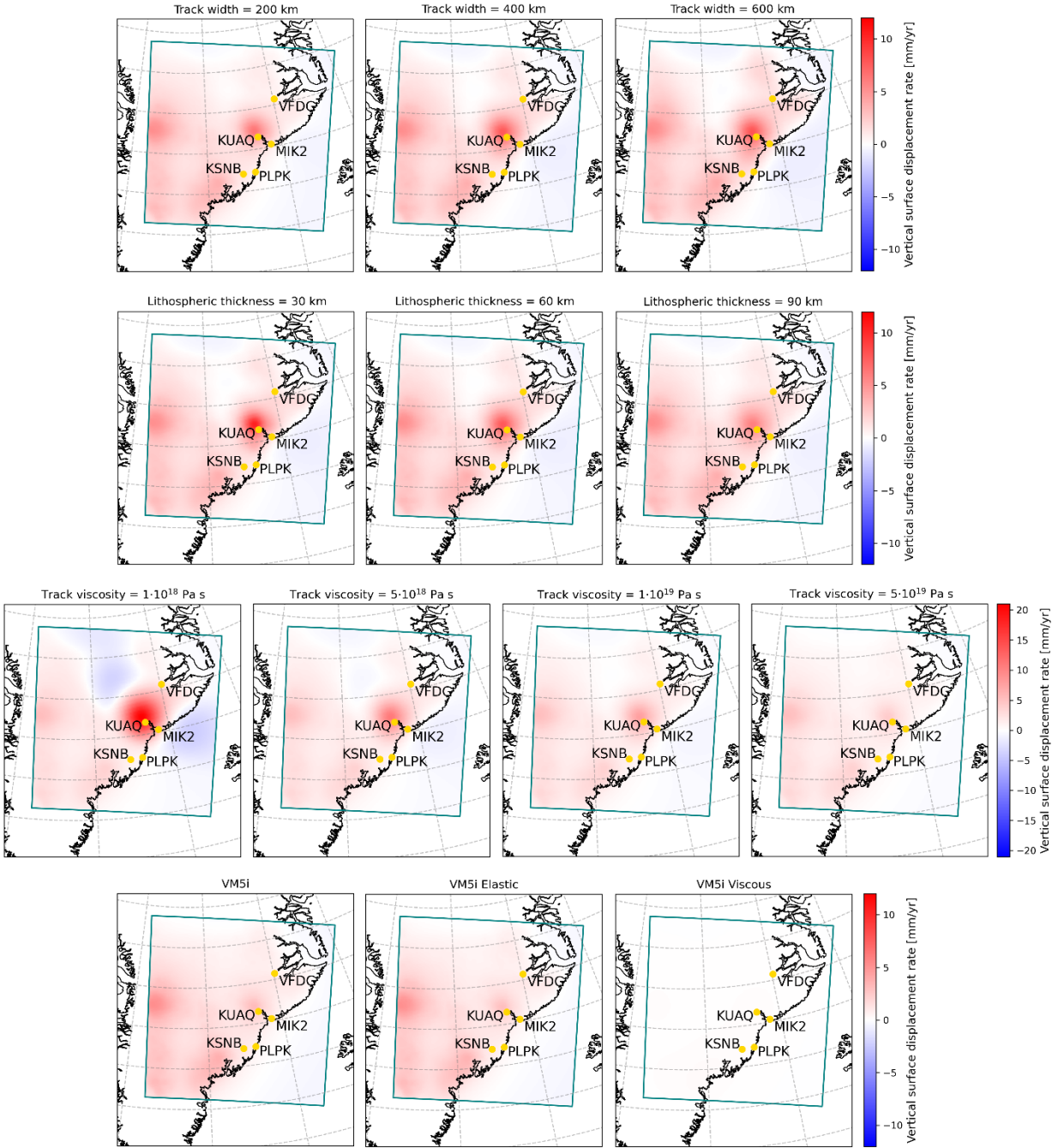
Fig. S8. Regional modelling of present-day uplift rates in response to satellite altimetry era ice loading changes within the ice loading area, for different plume track models.

Different Earth models are shown, as described in Fig. 4.
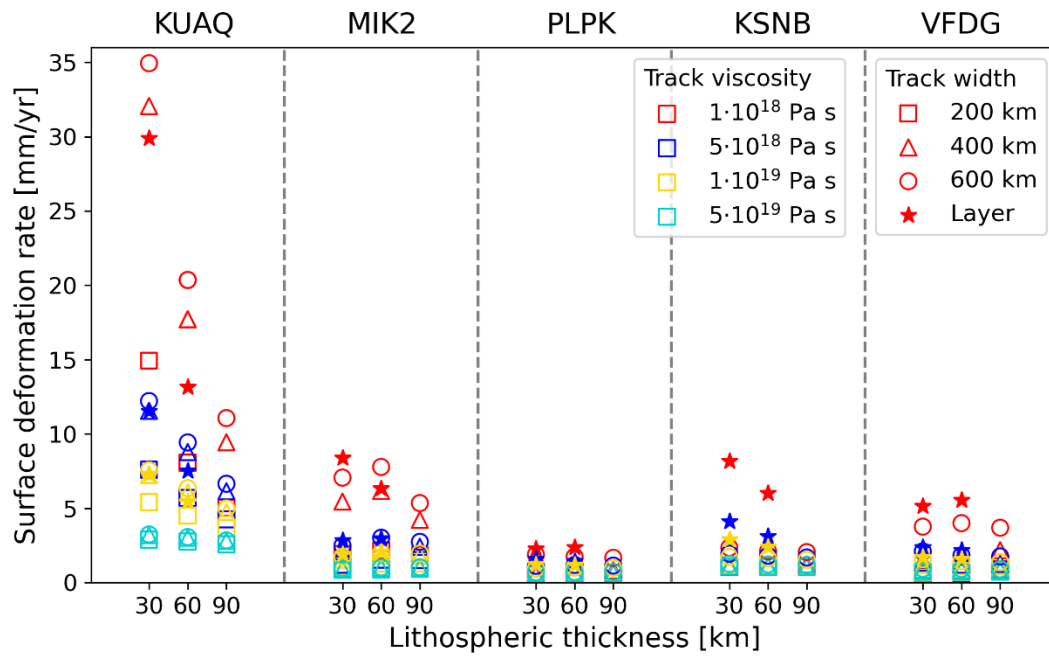
Fig. S9. Uplift rates at the five GNSS sites in response to satellite altimetry era ice loading changes (only), for all different plume track models.

Like Fig. 5, but showing uplift in response to satellite altimetry era ice loading changes.

Table S3. Rheological model VM5i

Earth model properties of the layered VM5i rheological model [2, 3, 1]. LT, UM, TZ, and LM stand for lithosphere, upper mantle, transition zone, and lower mantle, respectively.

Layer	Lower radius r_- (km)	Upper radius r_+ (km)	Density ρ (kg m^{-3})	Shear modulus μ (Pa $\cdot 10^{11}$)	Viscosity η (Pa s $\cdot 10^{21}$)
LT	6281.000	6371.000	3192.800	0.596	∞
UM1	6151.000	6281.000	3369.058	0.667	0.5
UM2	5971.000	6151.000	3475.581	0.764	0.5
TZ	5701.000	5971.000	3857.754	1.064	0.5
LM1	5401.000	5701.000	4446.251	1.702	1.5
LM2	5072.933	5401.000	4615.829	1.912	3.2
LM3	4716.800	5072.933	4813.845	2.124	3.2
LM4	4332.600	4716.800	4997.859	2.325	3.2
LM5	3920.333	4332.600	5202.004	2.554	3.2
LM6	3480.000	3920.333	5408.573	2.794	3.2
Core	N/A	3480.000	10931.731	0	0
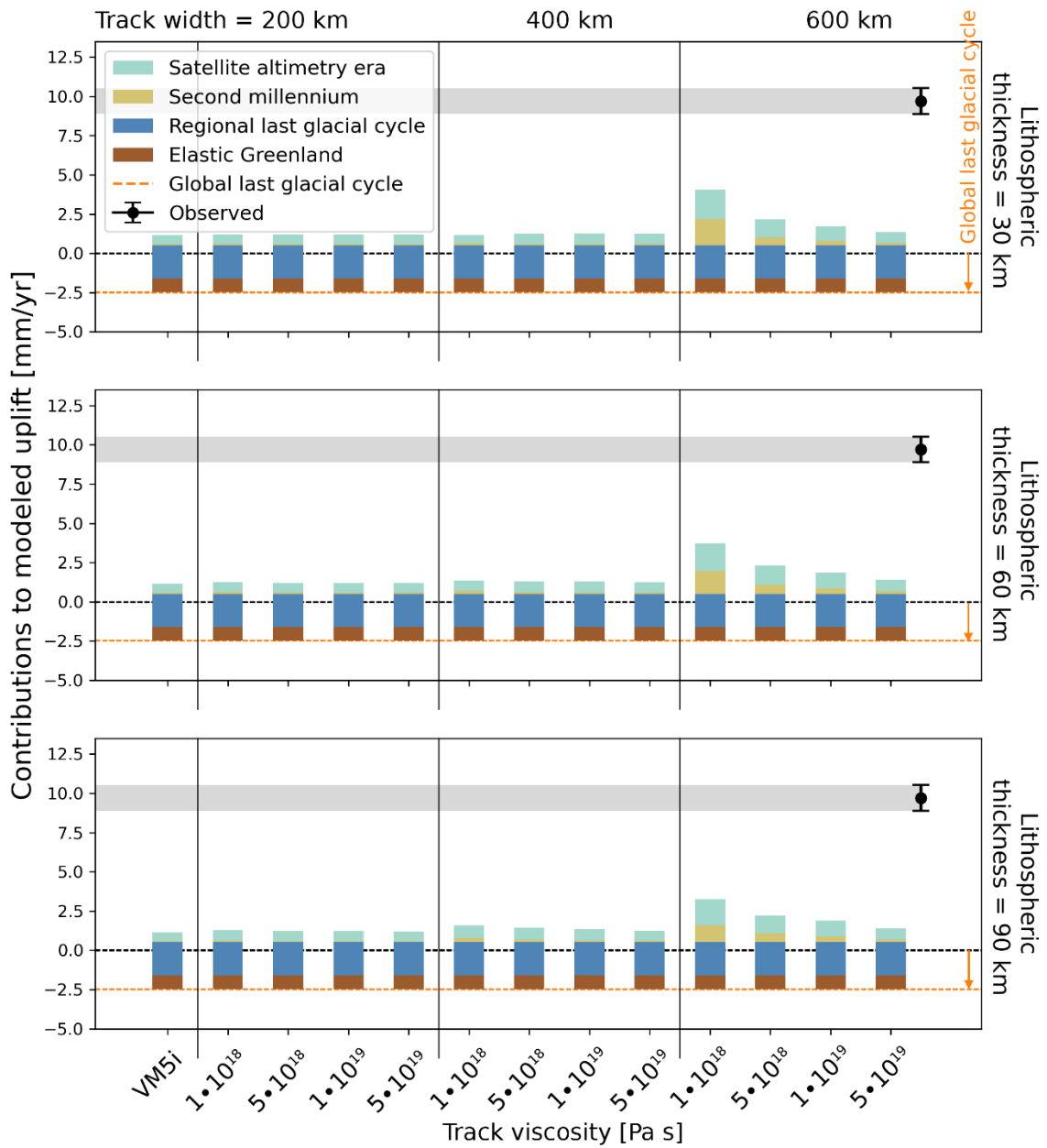
Fig. S10. Individual contributions to uplift rates at PLPK for different plume track models. Like Fig. 6, but for the PLPK GNSS site.
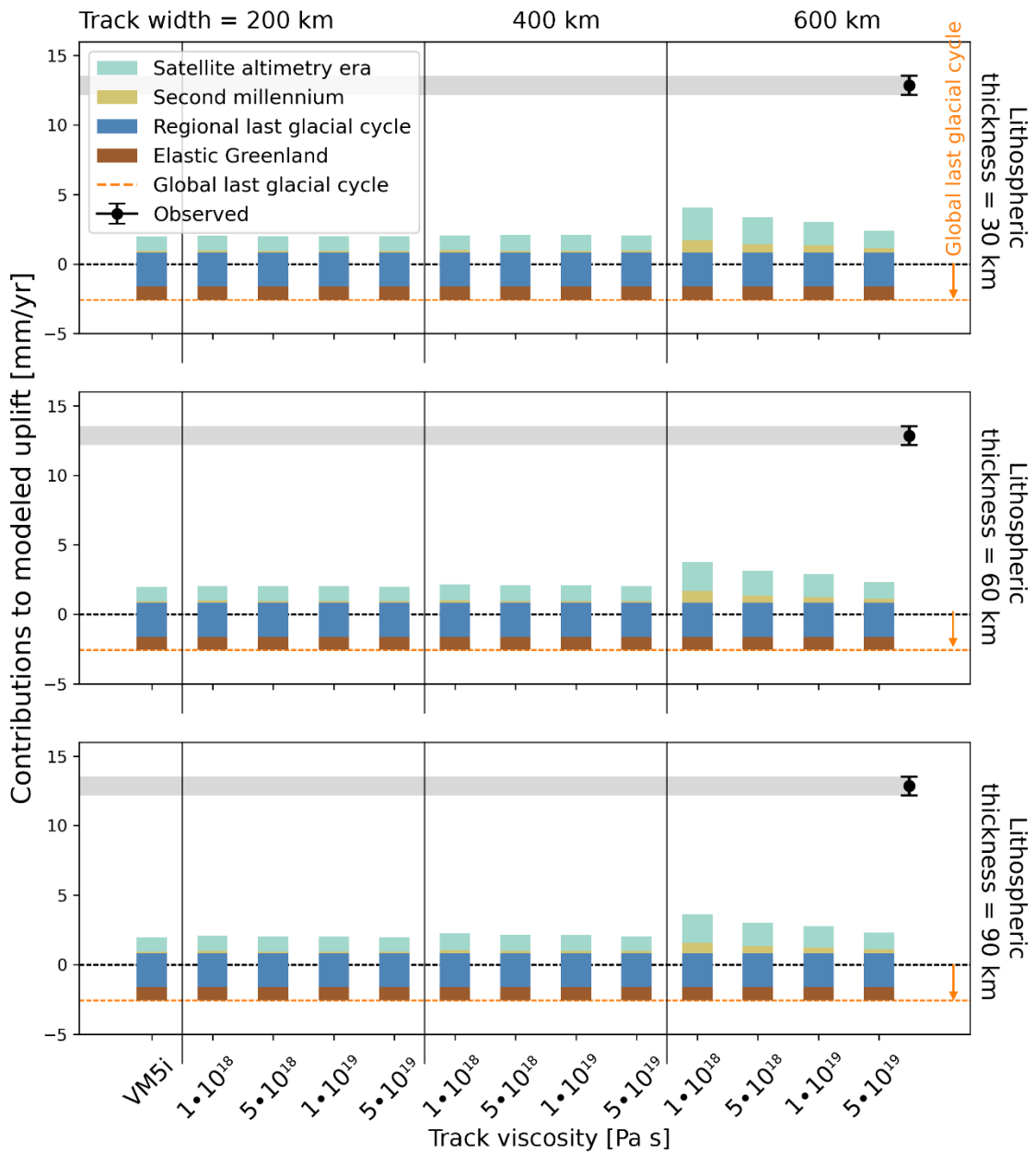
Fig. S11. Individual contributions to uplift rates at KSNB for different plume track models.
Like Fig. 6, but for the KSNB GNSS site.
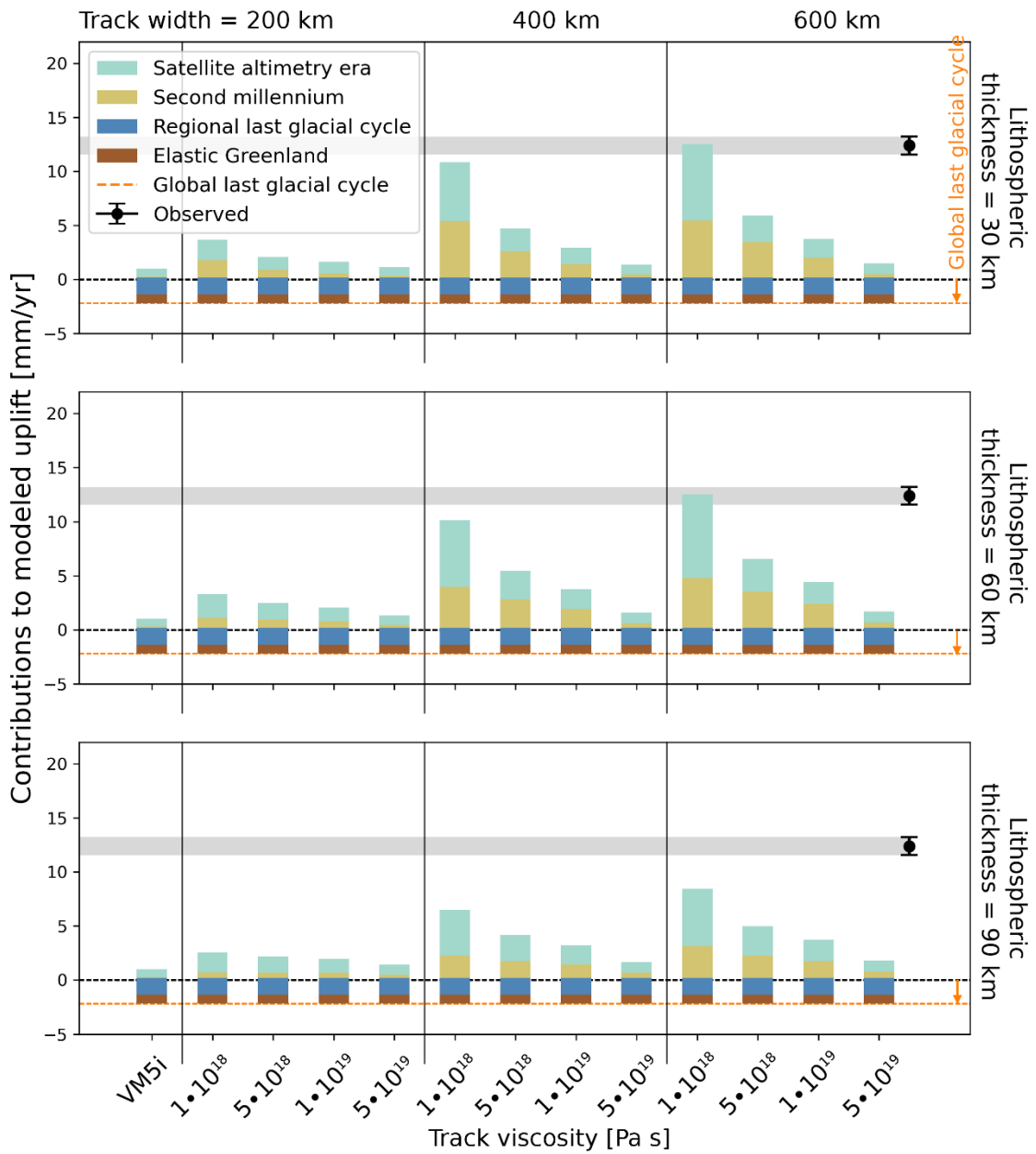
Fig. S12. Individual contributions to uplift rates at MIK2 for different plume track models.
Like Fig. 6, but for the MIK2 GNSS site.
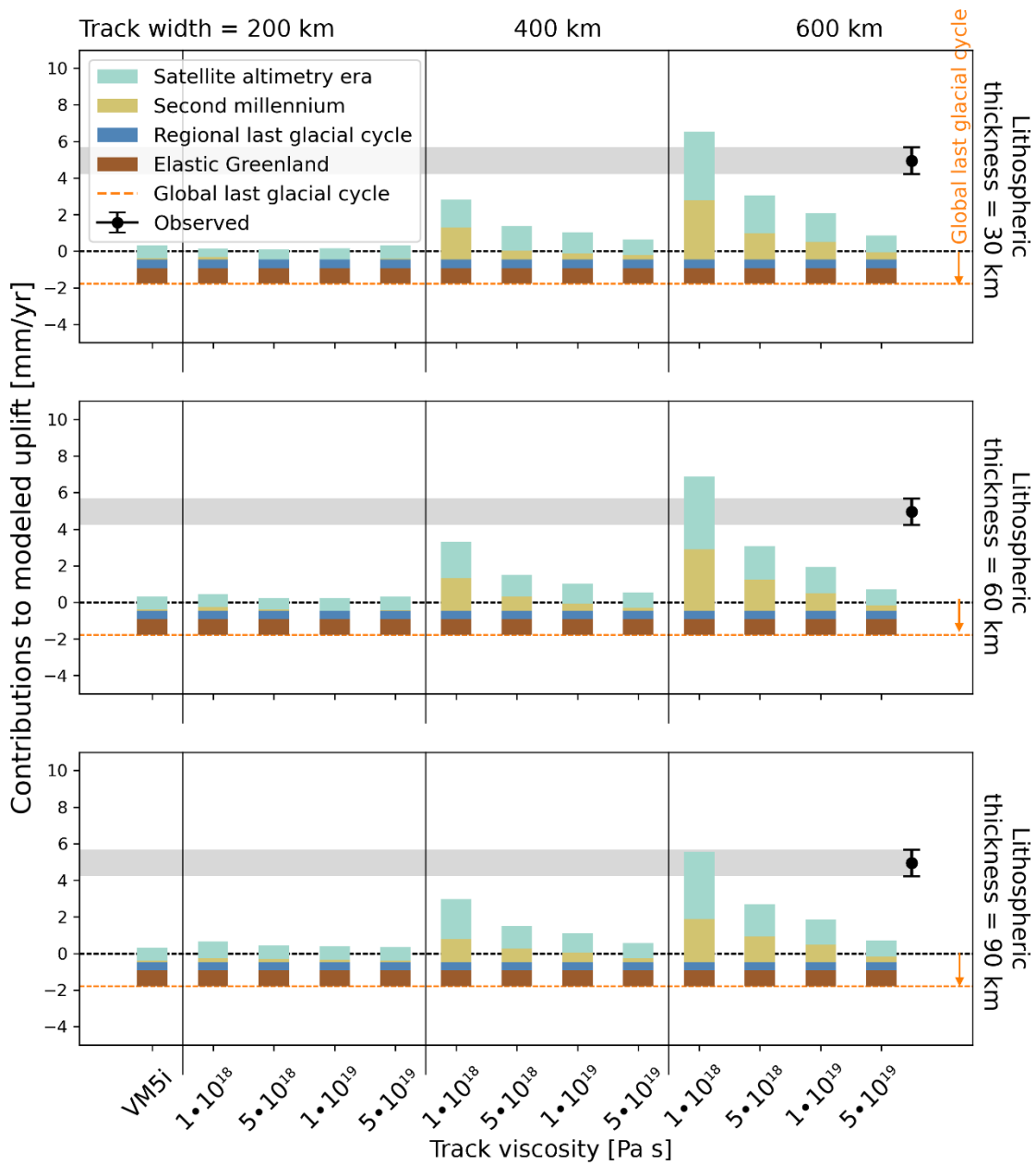
Fig. S13. Individual contributions to uplift rates at VFDG for different plume track models.
Like Fig. 6, but for the VFDG GNSS site.
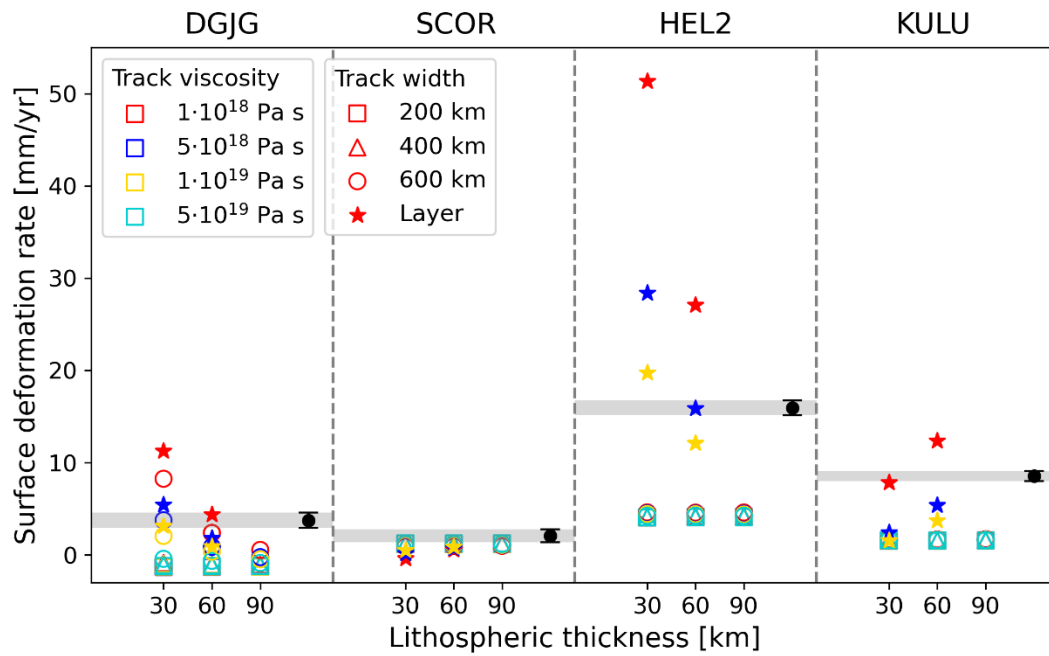
Fig. S14. Total uplift rates at four GNSS sites for different plume track models.
Like Fig. 5, but for the DGJG, SCOR, HEL2, and KULU GNSS sites.
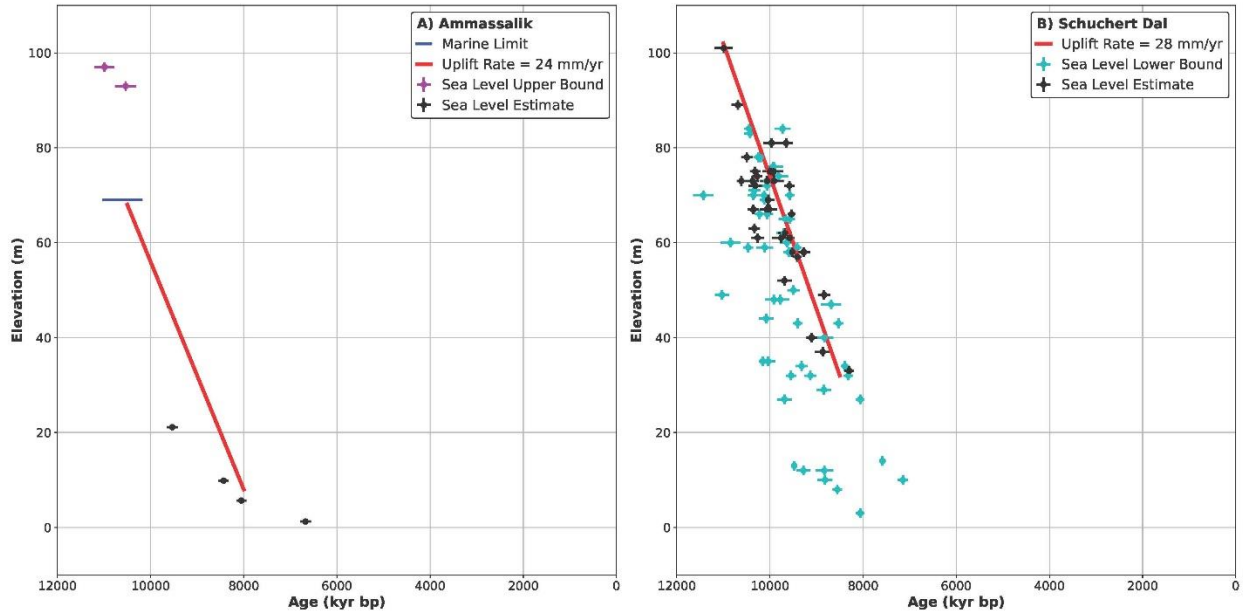
Fig. S15. Indicators for Holocene relative sea level change for sites in Southeast Greenland (**A**) for Ammassalik (Am) as compiled by *Long et al.* (2008) [4] and (**B**) for Schuchert Dal (SD) as compiled by *Hall et al.* (2010) [5]. See Figs. 1B and 7C for the locations of these sites. Shown are measurements of the age (in ka bp) and elevation (in m) of indicators of past sea level, for direct indexes of sea level shown (black), marine-based indicators that provide a lower bound (cyan), and terrestrial-based indicators that provide an upper bound (magenta), with uncertainties (vertical and horizontal bars), inferred average rate (red line), and a marine limit at Ammassalik (blue bar).
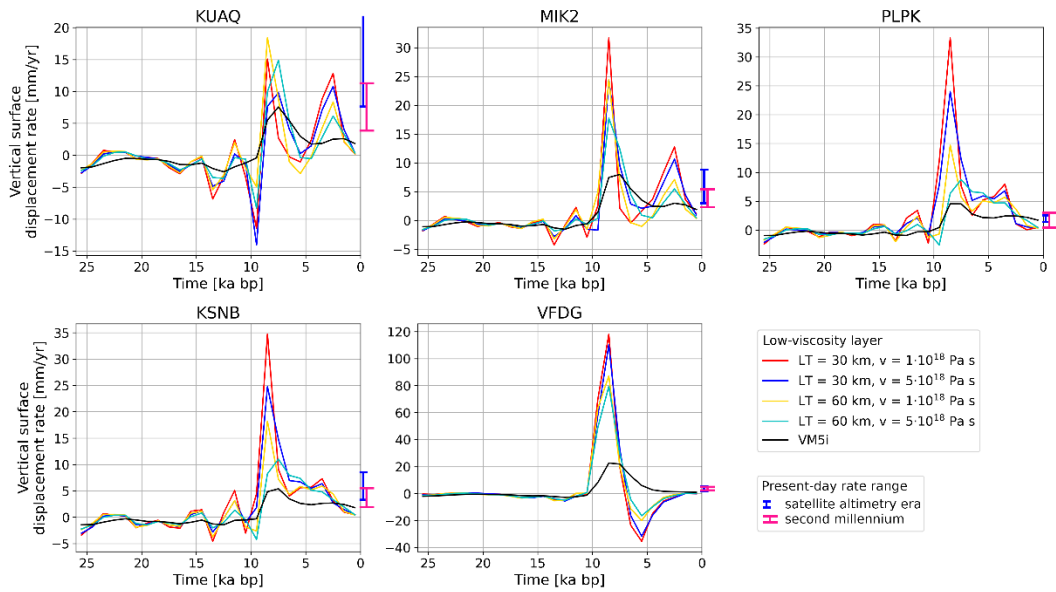
Fig. S16. Uplift rates due to last glacial cycle ice loading, for different low-viscosity layer models.

Vertical surface displacement rates since the last glacial maximum for low-viscosity layers of $1 \cdot 10^{18}$ and $5 \cdot 10^{18}$ Pa s, and nominal lithospheric thicknesses of $T_{LT} = 30$ and 60 km (see legend) for five GNSS sites. Shown for comparison are results for the layered VM5i rheological model (black), ranges of present-day rates induced by ice loading changes over the satellite altimetry era (blue bar) and second millennium (pink bar). Note that these low-viscosity layer models are constructed using a plume track that is wider than the model itself. Because the lithospheric thickness is reduced by 25% within the plume track (Fig. 1C), the $T_{LT} = 30$ and 60 km models use effective lithospheric thicknesses of 22.5 and 45 km, respectively.

19
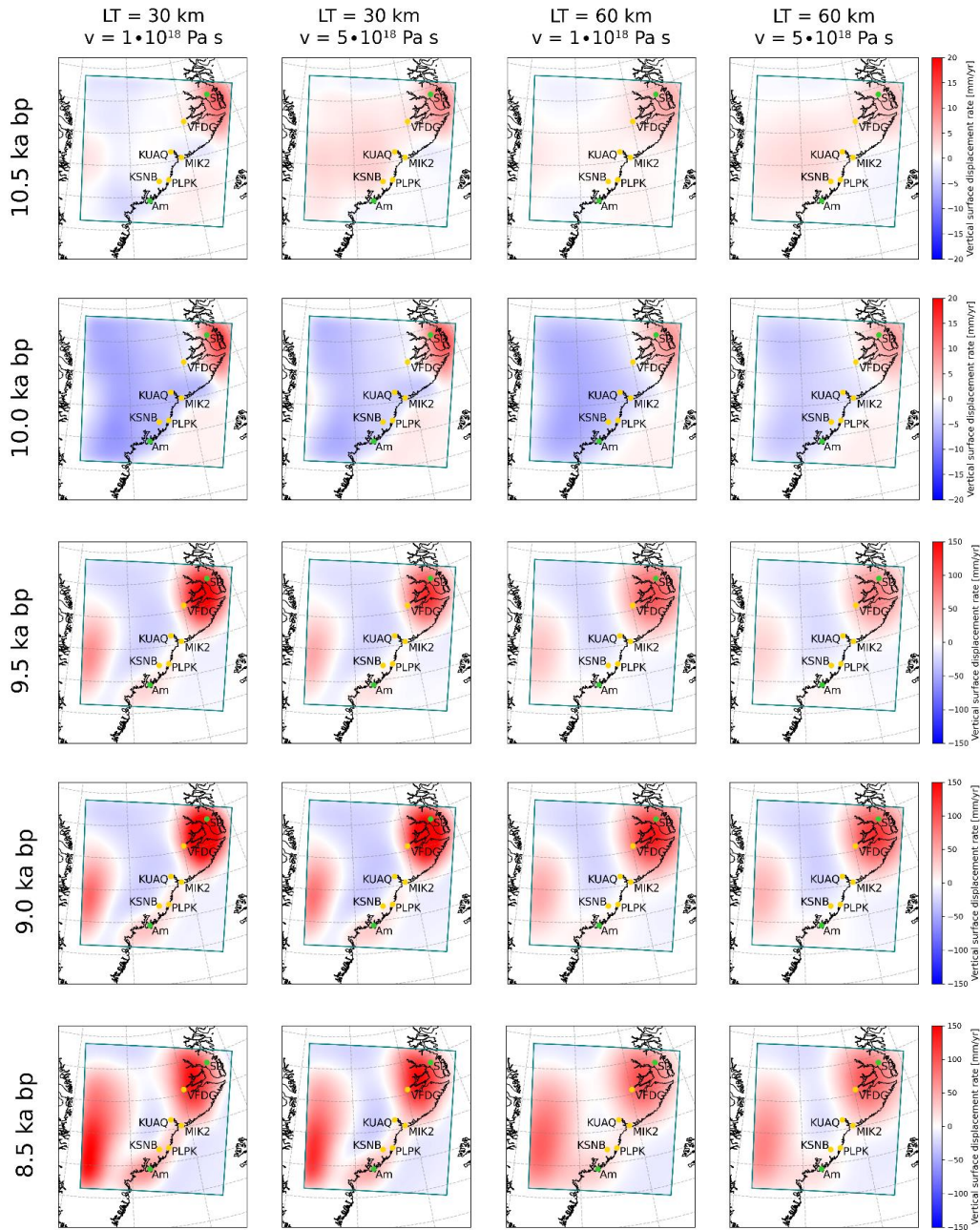
Fig. S17. Last deglaciation uplift rates in southeast Greenland
Shown for Earth models with low-viscosity layers of $1 \cdot 10^{18}$ and $5 \cdot 10^{18}$ Pa s and nominal lithospheric thicknesses of $T_{LT} = 30$ and 60 km (see column headers). Note that these models are constructed using a plume track that is wider than the model itself. Because the lithospheric thickness is reduced by 25% within the plume track (Fig. 1C), the $T_{LT} = 30$ and 60 km models use effective lithospheric thicknesses of 22.5 and 45 km, respectively.
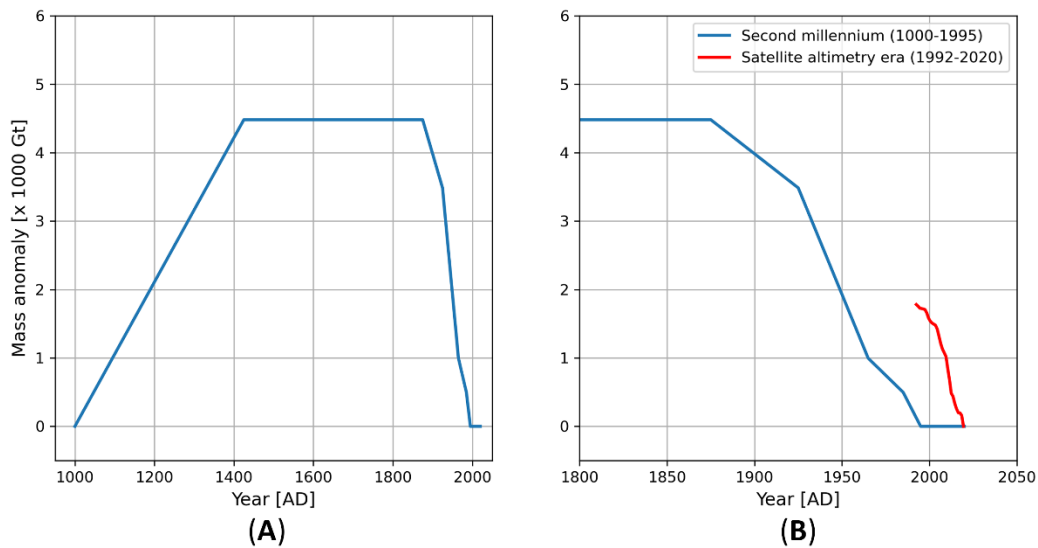
Fig. S18. Mass anomaly during the second millennium (1000-1995) within the ice loading area in southeast Greenland.

(**A**) Mass anomaly based on the Bayesian inference estimate from Adhikari *et al.* [6] for glacial volumes during the Little Ice Age, with the mass anomaly set to zero at 1000 AD. The mass loading is zero again at 1995 AD, after which the simulation runs until 2020 with zero loading. (**B**) Same as in (**A**) but from 1800 AD, and with the mass anomaly changes during the satellite altimetry era (red). There is a 3-year overlap between the second millennium and satellite altimetry datasets (1992-1995). However, the ice mass loss during this short overlap period is less than 5% of the total over the satellite altimetry era (red line) and less than 3.5% of the total second millennium period (blue line).
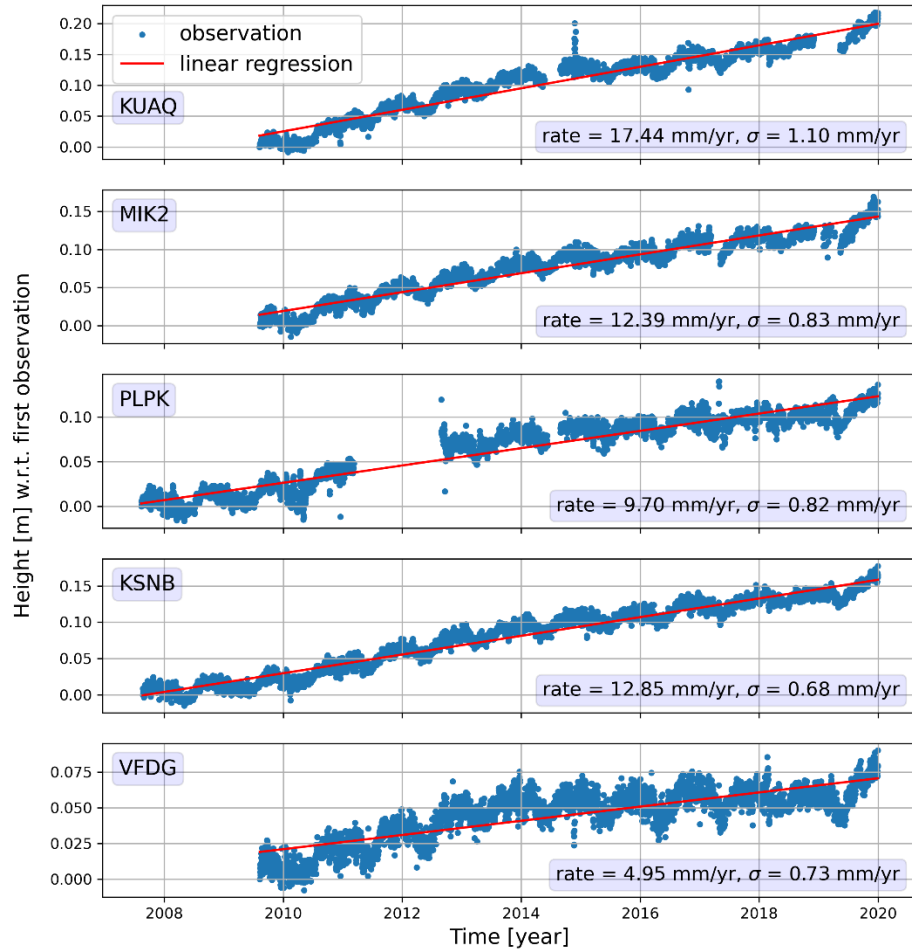
Fig. S19. GNET GNSS station height observations in southeast Greenland with linear regression.

GNSS station height observations (blue dots) at the five stations (KUAQ, MIK2, PLPK, KSNB, and VFDG) [7, 8, 9, 10, 11] in the area of interest in southeast Greenland (Fig. 1B) as a function of time, from the start of observations until 31-12-2019 (end of the VMB data), with linear regression (red line) and standard deviation of the detrended data. Individual height observations with respect to a reference position with a standard deviation larger than 0.1 m are removed before the linear regression analysis.
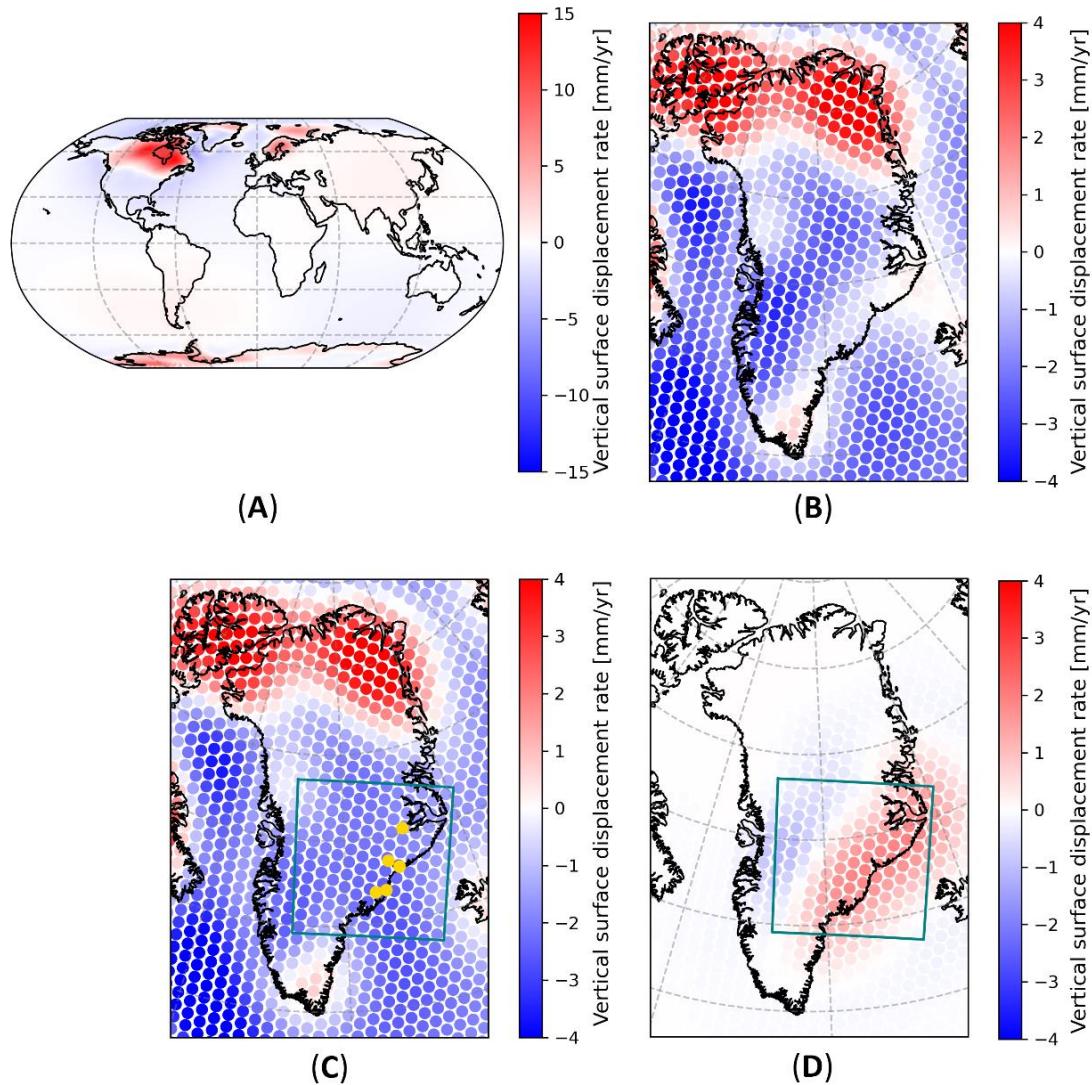
Fig. S20. Present-day uplift rates in response to global last glacial cycle ice loading.
(**A**) Global vertical displacement rates in response to ice loading changes over the last glacial cycle, computed using SELEN [1] for the ICE-6G_C(VM5a) ice history and Earth model [2, 3]. (**B**) The same as in (**A**), but zoomed in to Greenland. (**C**) The same as in (**B**), but excluding ice loading inside of our ice loading area in southeast Greenland (teal box) and with the five GNSS sites of interest (yellow dots). (**D**) The same as in (**B**), but for only the ice loading inside of our ice loading area in southeast Greenland (as for Fig. S1A).
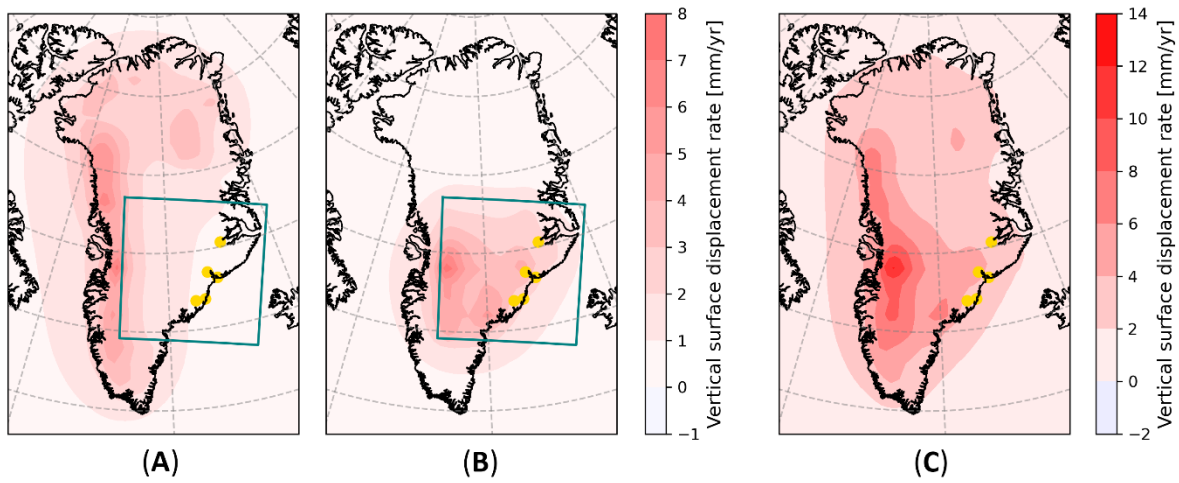
Fig. S21. Elastic uplift rates in response to the satellite altimetry era ice loading changes across Greenland.

Elastic vertical surface displacement rates for **(A)** ice loading outside of the ice loading area (teal box), **(B)** for ice loading inside of the ice loading area, and **(C)** for all the ice loading across Greenland. GNSS sites are shown by yellow dots.
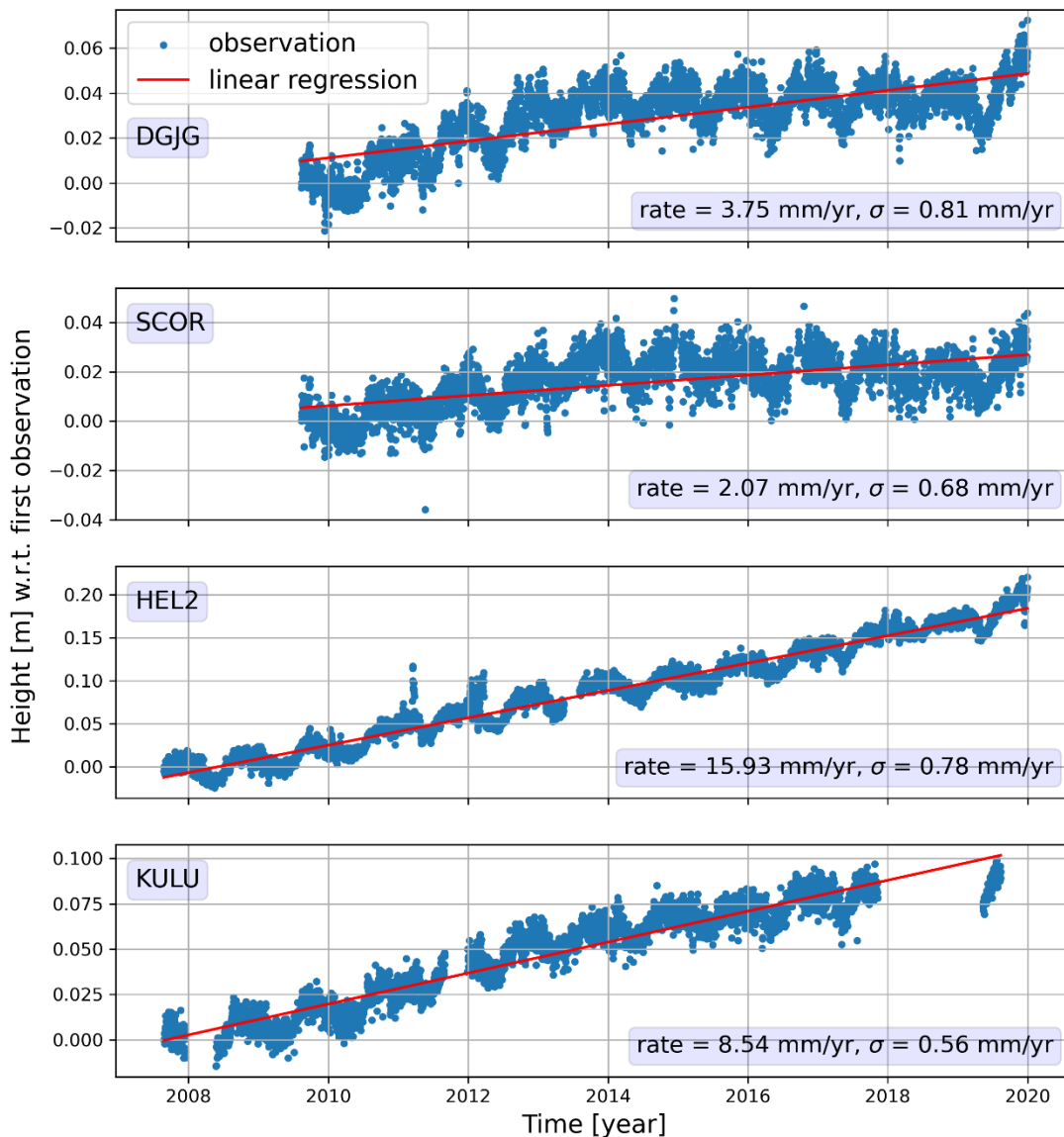
Fig. S22. GNET GNSS station height observations in southeast Greenland with linear regression.

GNSS station height observations (blue dots) at the four stations (DGJG, SCOR, HEL2, and KULU) [12, 13, 14, 15] outside the area of interest but inside the ice loading area in southeast Greenland (Fig. 7B), as a function of time until 31-12-2019 (end of the VMB data), with linear regression (red line) and standard deviation of the detrended data. Individual height observations with respect to a reference position with a standard deviation larger than 0.1 m are removed before the linear regression analysis.

Supplementary References

[1]   G. Spada and D. Melini, "SELEN4 (SELEN version 4.0): a Fortran program for solving the gravitationally and," *Geoscientific Model Development,* vol. 12, no. 12, pp. 5055-5075, 2019, doi:10.5194/gmd-12-5055-2019.

[2]   D. F. Argus, W. R. Peltier, R. Drummond and A. W. Moore, "The Antarctica component of postglacial rebound model ICE-6G_C (VM5a) based upon GPS positioning, exposure age dating of ice thicknesses, and relative sea level histories," *Geophysical Journal International,* vol. 198, no. 1, pp. 537-563, 2014, doi:10.1093/gji/ggu140.

[3]   W. R. Peltier, D. F. Argus and R. Drummond, "Space geodesy constrains ice-age terminal deglaciation: The global ICE-6G_C (VM5a) model," *Journal of Geophysical Research: Solid Earth,* vol. 120, no. 1, pp. 450-487, 2015, doi:10.1002/2014JB011176.

[4]   A. J. Long, D. H. Roberts, M. J. Simpson, S. Dawson, G. A. Milne and P. Huybrechts, "Late Weichselian relative sea-level changes and ice sheet history in southeast Greenland," *Earth and Planetary Science Letters,* vol. 272, no. 1-2, pp. 8-18, 2008, doi:10.1016/j.epsl.2008.03.042.

[5]   B. L. Hall, C. Baroni and G. H. Denton, "Relative sea-level changes, Schuchert Dal, East Greenland, with implications for ice extent in late-glacial and Holocene times," *Quaternary Science Reviews,* vol. 29, no. 25-26, pp. 3370-3378, 2010, doi:10.1016/j.quascirev.2010.03.013.

[6]   S. Adhikari, G. A. Milne, L. Caron, S. A. Khan, K. K. Kjeldsen, J. Nilsson, E. Larour and E. R. Ivins, "Decadal to Centennial Timescale Mantle Viscosity Inferred From Modern Crustal Uplift Rates in Greenland," *Geophysical Research Letters,* vol. 48, no. 19, p. e2021GL094040, 2021, doi:10.1029/2021GL094040.

[7]   The Danish Agency SDFE, UNAVCO Community and M. Bevis, *Greenland GNSS Network - KUAQ-Kangerdlussuaq Gletscher P.S.,* GPS/GNSS Observations Dataset: The GAGE Facility operated by EarthScope Consortium, 2009, doi:10.7283/HQ0D-3D69.

[8]   The Danish Agency SDFE, UNAVCO Community and M. Bevis, *Greenland GNSS Network - MIK2-Mikis Fjord P.S.,* GPS/GNSS Observations Dataset: The GAGE Facility operated by EarthScope Consortium, 2009, doi:10.7283/ABT9-NF76.

[9]   The Danish Agency SDFE, UNAVCO Community and M. Bevis, *Greenland GNSS Network - PLPK-Pilappik P.S.,* GPS/GNSS Observations Dataset: The GAGE Facility operated by EarthScope Consortium, 2007, doi:10.7283/QQJP-4H93.

[10] The Danish Agency SDFE, UNAVCO Community and M. Bevis, *Greenland GNSS Network - KSNB-Steenstrup Nordre Brae P.S.,* GPS/GNSS Observations Dataset: The GAGE Facility operated by EarthScope Consortium, 2007, doi:10.7283/RHVV-9P67.

[11] The Danish Agency SDFE, UNAVCO Community and M. Bevis, *Greenland GNSS Network - VFDG-Vestfjord Gletscher P.S.,* GPS/GNSS Observations Dataset: The GAGE Facility operated by UNAVCO, Inc., 2009, doi:10.7283/VT9V-WH52.

[12] The Danish Agency SDFE, UNAVCO Community and M. Bevis, *Greenland GNSS Network - DGJG-Daugaard Jensen Gletshcer P.S.,* GPS/GNSS Observations Dataset: The GAGE Facility operated by EarthScope Consortium, 2009, doi:10.7283/S3EH-XJ14.

[13] International GNNS Service (IGS), *Scoresbysund (SCOR),* 2009, url: https://gage-data.earthscope.org/archive/gnss/products/position/SCOR.

[14] The Danish Agency SDFE, UNAVCO Community and M. Bevis, *Greenland GNSS Network - HEL2-Helheim Glacier P.S,* GPS/GNSS Observations Dataset: The GAGE Facility operated by UNAVCO, Inc., 2007, doi:10.7283/7PB0-2Z53.

[15] The Danish Agency SDFE, UNAVCO Community, K. Larson and T. M. van Dam, *Greenland GNSS Network - KULU-Kulusuk P.S.,* GPS/GNSS Observations Dataset: The GAGE Facility operated by EarthScope Consortium, 1998, doi:10.7283/MF3E-KV11.